Structure of Supersonic Turbulent Flow Past a Sharp Fin

Doyle D. Knight*
Rutgers University, New Brunswick, New Jersey
C. C. Horstman†
NASA Ames Research Center, Moffett Field, California
and
Brian Shapey‡ and Seymour Bogdonoff§
Princeton University, Princeton, New Jersey

The three-dimensional shock wave-turbulent boundary-layer interaction generated by a sharp fin is examined both experimentally and theoretically at Mach 3 for a fin angle $\alpha_g = 20$ deg and Reynolds number $Re_{\delta_\infty} = 9 \times 10^5$. This study represents an extension of previous research for the sharp fin configuration to stronger interactions. The experimental data include surface pressure profiles, surface streamline patterns, and boundary-layer profiles of pitot pressure and yaw angle. Two separate theoretical approaches or "models" were employed. Both models utilize the three-dimensional compressible Navier-Stokes equations in mass-averaged variables. The theoretical approach of Knight employs the algebraic turbulent eddy viscosity model of Baldwin and Lomax, and the theoretical model of Horstman employs the two-equation turbulence model of Jones and Launder coupled with the wall function model of Viegas and Rubesin.

I. Introduction

THE focus of the present paper is the three-dimensional oblique shock wave-turbulent boundary-layer interaction generated by a sharp fin attached to a flat plate (Fig. 1). The overall flowfield is determined by the upstream Mach number M_∞, the Reynolds number Re_{δ_∞} based upon the boundary-layer thickness δ_∞ at the streamwise station corresponding to the leading edge of the fin (where δ_∞ is measured in the absence of the fin), the nature of the thermal boundary condition on the flat plate and fin (e.g., adiabatic or fixed temperature), and the fin angle α_g. This configuration has been the subject of several experimental and theoretical investigations.[1] Experiments have focused principally on surface measurements, and include the studies of Stanbrook,[2] McCabe,[3] Law,[4] Kubota and Stollery,[5] Zheltovodov,[6] Dolling,[7] and Goodwin.[8] In recent years, detailed boundary-layer measurements have been obtained by Peake,[9] Oskam, Vas, and Bogdonoff,[10] and McClure and Dolling.[11] Numerical simulations using the three-dimensional Reynolds-averaged Navier-Stokes equations have been performed principally at Mach 3, and include the studies of Horstman and Hung[12] and Knight.[13-15] These computations, summarized in Ref. 16, considered fin angles α_g up to 10 deg at Mach 3. The investigation of Horstman and Hung utilized the Escudier[17] turbulence model, while the later work of Horstman[18] employed the Jones-Launder[19] model. The investigations of Knight utilized the Baldwin-Lomax[20] turbulence model. These studies examined the efficacy of the theoretical models through comparison with a wide variety of experimental data including surface pressure, skin friction, heat transfer, pitot pressure, yaw angle, pitch angle, and static pressure. In general, good agreement was obtained with the experimental data. Recently, a series of calculations have been performed by Horstman[21] at Mach 3 for $\alpha_g = 12$ deg to 20 deg, and the results compared with surface measurements (i.e., surface pressure and surface flow visualization) of Goodwin.[8]

There are three objectives for the present paper:

1) Examine the accuracy of the theoretical models for stronger interactions: The understanding of the efficacy of the theoretical models requires detailed comparison with experimental data for both surface and boundary-layer profiles. In the latter case, the strongest three-dimensional sharp fin interaction examined previously at Mach 3 corresponds to a pressure ratio $p_2/p_\infty = 2.01$ ($\alpha_g = 10$ deg), where p_∞ is the upstream static pressure and p_2 is the theoretical downstream inviscid pressure. In the present study, the theoretical models are examined for the three-dimensional sharp fin interaction at Mach 3 and $\alpha_g = 20$ deg, which exhibits a pressure rise of 3.7. This examination includes detailed comparison with experimental data for boundary-layer profiles of pitot pressure and yaw angle.

2) Comparison of two different theoretical models: An important objective of the present research is to examine the computed flowfields for the three-dimensional sharp fin interaction using two different turbulence models. In this effort, Navier-Stokes calculations have been performed by Knight and Horstman using the Baldwin-Lomax and Jones-Launder turbulence models, respectively. A principal issue is the determination of the sensitivity of the computed flowfield to the turbulence model employed.

3) Examine the flowfield structure of the three-dimensional sharp fin interaction: Provided the theoretical models yield good agreement with the experimental data for the Mach 3, $\alpha_g = 20$ deg configuration, the computed flowfields can be utilized to examine and understand the flowfield structure of this three-dimensional sharp fin interaction. Previous flowfield models, developed, for example, by Token,[22] and Kubota and Stollery,[5] may be examined using the computed flowfields.

Presented as Paper 86-0343, AIAA 24th Aerospace Sciences Meeting, Reno, NV, Jan. 6-9, 1986; received April 1, 1986; revision received Feb. 10, 1987.

*Professor, Department of Mechanical and Aerospace Engineering. Associate Fellow AIAA.
†Assistant Branch Chief, Associate Fellow AIAA.
‡Graduate Student, Department of Aerospace and Mechanical Engineering; presently at Rocketdyne, Inc., Canoga Park, CA.
§Professor, Department of Aerospace and Mechanical Engineering. Fellow AIAA.

II. Description of Experiment

The experiments were performed in the supersonic high Reynolds number wind tunnel at the Princeton University Gas Dynamics Laboratory. The facility has a 20 cm × 20 cm test section, with a nominal freestream Mach number of 2.93. The settling chamber pressure and temperature were 6.8×10^5 Pa ±1% and 251 K ±5%, respectively. The boundary-layer thickness δ_∞ at the apex of the fin is 1.4 cm, yielding a Reynolds number $Re_{\delta\infty} = 9.8 \times 10^5$. The experiments were performed under near adiabatic wall conditions.

The sharp fin is 14.21 cm long and 12.7 cm high. The fin was fabricated from aluminum with a sharp unswept leading edge, and oriented at a right angle to the tunnel wall (flat plate). The fin was mounted in a unique variable-geometry apparatus which permitted the achievement of fin angles exceeding 20 deg, thereby extending the range of the experiments beyond the earlier fixed-geometry configuration.[10]

Surface pressure distributions were obtained along rows of orifices aligned with the x direction. A kerosene-lampblack technique[23] was employed to obtain surface flow angularity. The boundary layer on the tunnel wall (flat plate) was surveyed using a computer-controlled nulling cobra probe[11] which measured pitot pressure p_p and yaw angle β, where $\beta = \tan^{-1}(w/u)$ with (u, v, w) indicating the Cartesian velocity components in the (x, y, z) coordinate system (Fig. 1). The survey locations,[16] shown in Fig. 2, were selected to provide detailed information within the region between the line of coalescence (three-dimensional separation line)[9] and the shock wave, and the region downstream of the shock. The incoming flow on the tunnel wall is an equilibrium, two-dimensional boundary layer which has been extensively surveyed[10,11] and observed to closely fit the Law of the Wall and Wake.

III. Description of Computations

The governing equations are the full mean compressible three-dimensional Navier-Stokes equations using mass-averaged variables and strong conservation form.[13] The molecular dynamic viscosity is given by Sutherland's law. The molecular and turbulent Prandtl numbers are 0.73 and 0.9, respectively. Two separate turbulence models are employed, namely, the Baldwin-Lomax (BL) algebraic model[20] and the Jones-Launder (JL) two-equation model.[19] In the latter case, the model incorporates the compressible wall functions of Viegas and Rubesin.[24,25]

The computational domain is shown in Fig. 1. The freestream conditions were chosen to closely match the experimental configuration. The total pressure $p_{t\infty} = 690$ kPa for both models, and the total temperature $T_{t\infty} = 256$ and 267 deg K, respectively, for the Baldwin-Lomax and Jones-Launder models. On the upstream boundary ABHG, the flow variables are held fixed at values obtained from a boundary-layer solution which matched the experimental momentum thickness. The boundary-layer thickness at the apex was 1.3 cm for the Baldwin-Lomax model and 1.4 cm for the Jones-Launder model. On the solid surfaces ABCDEF and FEKL, the velocity is zero, a fixed temperature (near adiabatic) is applied, and the normal derivative of the static pressure is set to zero. On the symmetry boundary AFLG, the normal component of the velocity is set to zero, and the normal derivatives of the remaining flow quantities are assumed to be zero. On the right boundary BCDJIH, the gradient of the flow variables in the z direction is set to zero. The width of the domain is sufficient to ensure the shock wave passes through the downstream boundary EDJK, where the streamwise gradients of the flow variables are set to zero. On the upper surface GHIJKL, the normal component of the flow variables is set to zero.

The computations employing the Baldwin-Lomax model were solved by an efficient hybrid explicit-implicit numerical algorithm[13] on the VPS-32 at NASA Langley Research Center. The VPS-32 is a vector-processing computer which is similar to the CYBER 205. The calculations using the Jones-Launder model were solved using the explicit numerical algorithm of MacCormack[26] on the Cray X-MP/24 at the NASA Ames Research Center. The calculations employed a total of 64,956 grid points for the Baldwin-Lomax model, and 90,112 points for the Jones-Launder model. Details of the grid resolution are provided in Ref. 16.

IV. Results

A. Comparison with Experiment

The computed upstream boundary-layer profiles, matched to the experimental momentum thickness at the apex of the fin, provided good agreement with the experimental pitot pressure at station 2, and even at stations downstream of the line of coalescence, i.e., stations 3, 4, and 9 in Fig. 2. In Fig. 3, the computed and experimental pitot pressure profiles are displayed at station 5, located at $x_s = x - x_{\text{shock}} = -1.4\delta_\infty$ and $z = 5.8\delta_\infty$, where x_{shock} is the location of the theoretical inviscid shock at the specified spanwise location z. The station

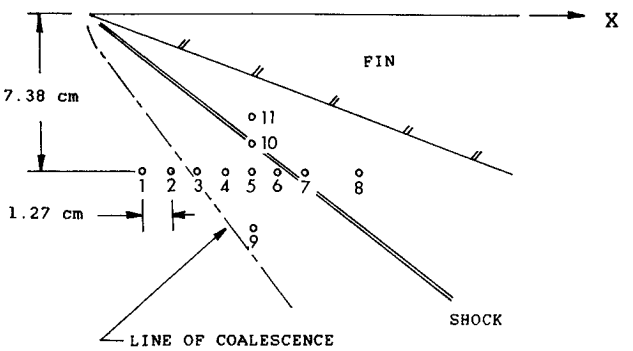

Fig. 2 Location of experimental surveys.

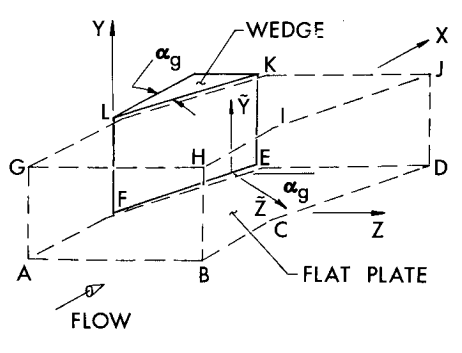

Fig. 1 Physical region for three-dimensional sharp fin.

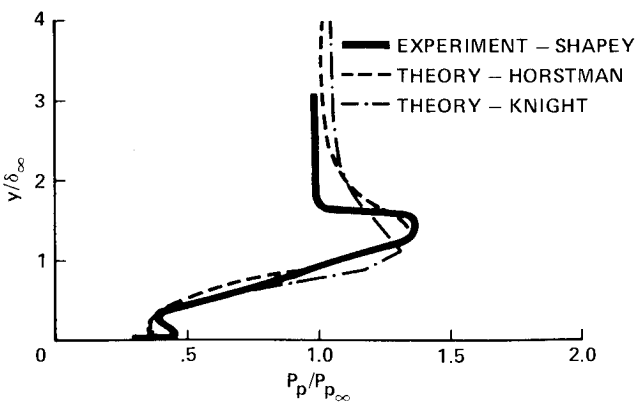

Fig. 3 Pitot pressure at station 5.

is approximately two-thirds of the distance between the line of coalescence and the theoretical inviscid shock at this spanwise position. The horizontal axis is the pitot pressure p_p, normalized by the upstream freestream pitot pressure $p_{p\infty}$. The vertical axis is the distance measured from the flat plate, normalized by the upstream boundary-layer thickness δ_∞. The experimental profile displays a slight undershoot in the pitot pressure at $y = 0.3\delta_\infty$. The computed profiles are in reasonable agreement with the experimental data, and accurately predict the observed overshoot in p_p. The shock-capturing nature of both numerical algorithms can be seen in the smearing of the pitot pressure profile near $y = 1.5\delta_\infty$.

In Fig. 4, pitot pressure profiles are displayed at station 7, located at $x_s = 0.6\delta_\infty$ and $z = 5.8\delta_\infty$, slightly behind the shock wave. Good agreement is again observed. Both computed and experimental profiles exhibit a distinct undershoot in the pitot pressure at $y = .4\delta_\infty$. This phenomenon is associated with the existence of a large vortical structure (see Sec. IV C). The discrepancy in the computed pitot pressure outside the boundary layer is associated with the shock-capturing nature of the numerical algorithms, the difference in streamwise grid spacing for the two computations, and the proximity of station 7 to the shock. Note that the freestream pitot pressure downstream of the shock wave exceeds the upstream freestream pitot pressure. In Fig. 5, results are shown at station 8, located furthest downstream of the shock at $x_s = 2.6\delta_\infty$ and $z = 5.8\delta_\infty$. The comparison between computed and experimental results is good. Additional profiles are presented in Ref. 16.

The computed and experimental yaw angle profiles at station 5, located approximately two-thirds of the distance between the line of coalescence and the shock wave at this spanwise position, are displayed in Fig. 6. The agreement between the theory and experiment is good, although the Jones-Launder model overpredicts the yaw angle in the outer portion of the boundary layer. The computed surface yaw angles are 61 deg (BL) and 53 deg (JL), in reasonable agreement with the experimental value of 60 deg.

The calculated and experimental yaw angle profiles at station 7, located immediately downstream of the shock, are shown in Fig. 7. The calculated results are again observed to be in close agreement with experiment, although displaying a somewhat less full profile near the surface. The predicted surface yaw angles are 61 deg (BL) and 59 deg (JL), in close agreement with the experimental value of 64 deg. In Fig. 8, yaw angle profiles are shown at station 8, downstream of the shock. The calculated and experimental profiles are observed to be in excellent agreement. The predicted surface values of 52 deg (BL) and 50 deg (JL) are in close agreement with the experimental value of 48 deg. Additional profiles are presented in Ref. 16.

In Fig. 9, the calculated surface pressure for both models is compared with the experimental data of Goodwin[8] for the same configuration at $z = 6.8\delta_\infty$. Both models accurately pre-

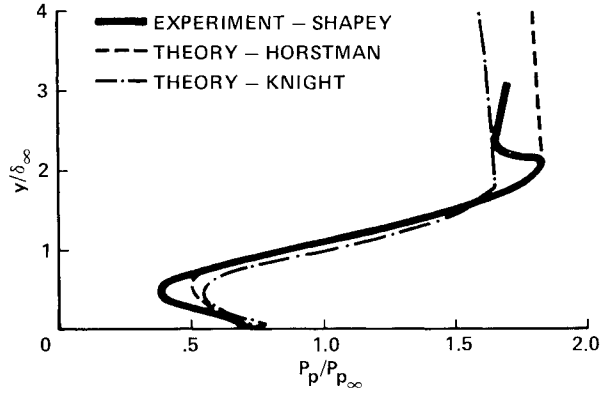

Fig. 4 Pitot pressure at station 7.

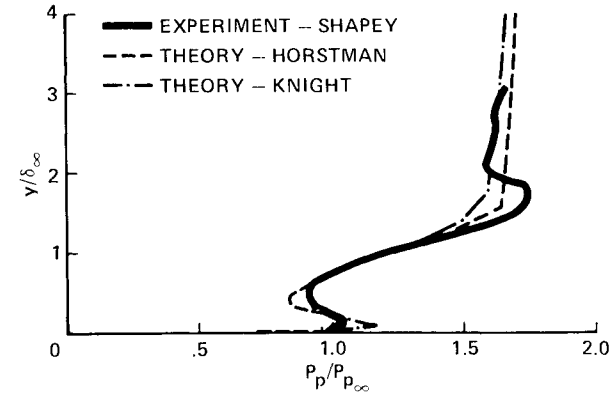

Fig. 5 Pitot pressure at station 8.

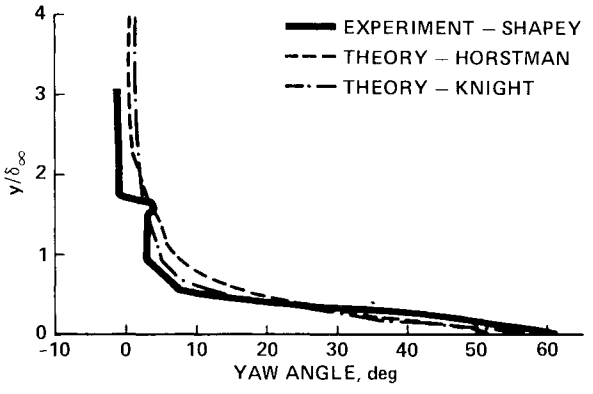

Fig. 6 Yaw angle at station 5.

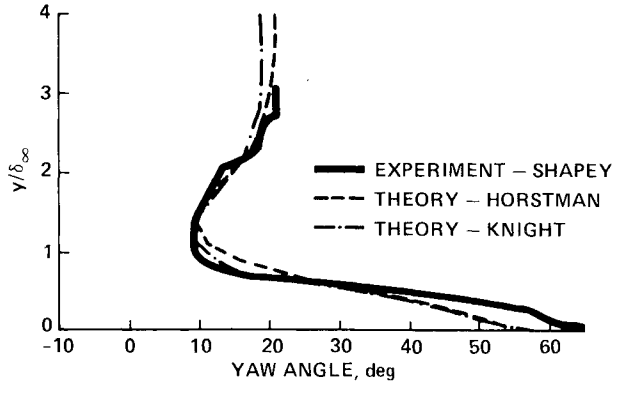

Fig. 7 Yaw angle at station 7.

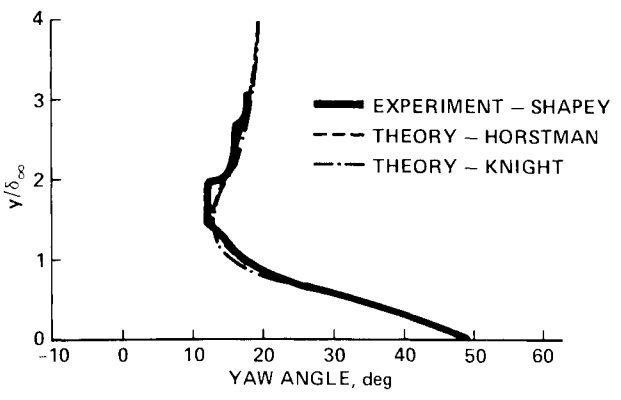

Fig. 8 Yaw angle at station 8.

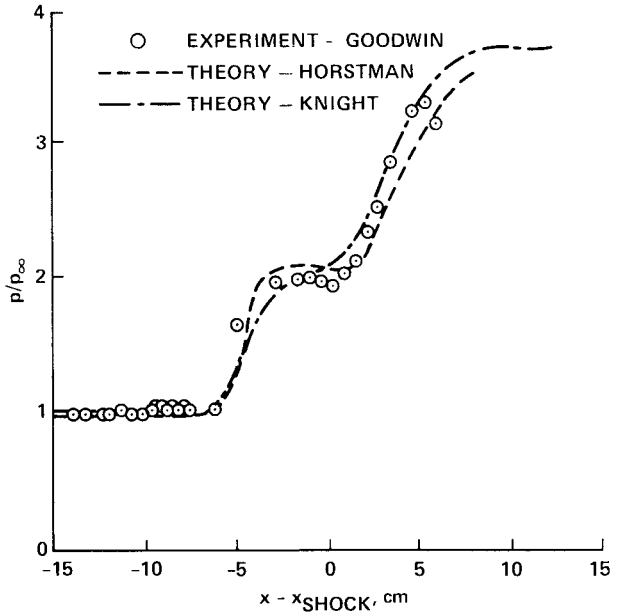

Fig. 9 Surface pressure at $z = 6.8\delta_\infty$.

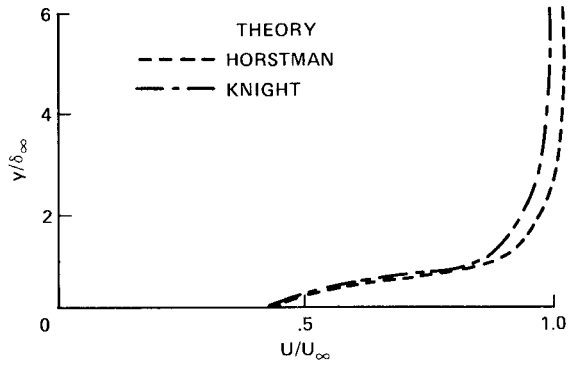

Fig. 10 Computed velocity in x direction at $x = 11\delta_\infty$, $z - z_{fin} = 6\delta_\infty$.

dict the extent of the upstream influence, and the overall pressure distribution. However, this close agreement is not necessarily observed for all three-dimensional sharp fin interactions. In particular, computations by Horstman[21] at Mach 3 for $\alpha = 14$ to 18 deg and $Re_{\delta_\infty} = 2.2 \times 10^5$ exhibit significant quantitative differences in the surface pressure distribution in comparison with experiment (e.g., differences of 25% in the plateau pressure), although displaying close agreement with the measured upstream influence.

B. Further Comparison of Computed Flowfield

A detailed comparison of the computed flowfields of Knight and Horstman was performed to determine the global extent of similarity of the two theoretical approaches. Profiles of the computed x-component velocity, yaw angle, pitch angle $\gamma = \tan^{-1}(v/\sqrt{u^2 + w^2})$, pitot pressure, Mach number, and turbulent eddy viscosity were examined at a selected stream-wise station $x = 11\delta_\infty$ for $z - z_{fin} = \delta_\infty$ to $10\delta_\infty$ in increments of δ_∞, where z_{fin} is the width of the fin at a given x. A representative sample is displayed in Figs. 10–13, corresponding to $x = 11\delta_\infty$ and $z - z_{fin} = 6\delta_\infty$. The position is roughly halfway between the line of coalescence and the shock wave (as measured in the stream-wise direction) at this spanwise location. The x-component velocity, yaw angle and pitch angle profiles, shown in Figs. 10, 11, and 12, respectively, are observed to be in very close agreement. Differences in the computed yaw angle occur only within the region $y < 0.3\delta_\infty$.

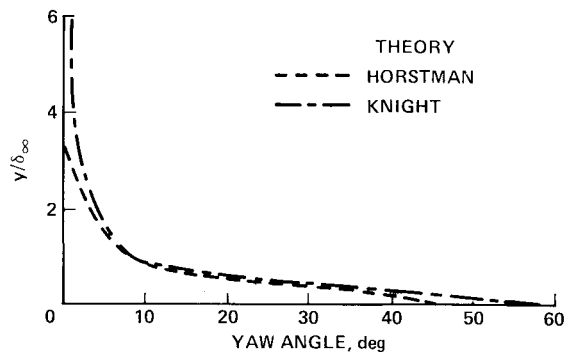

Fig. 11 Computed yaw angle in x direction at $x = 11\delta_\infty$, $z - z_{fin} = 6\delta_\infty$.

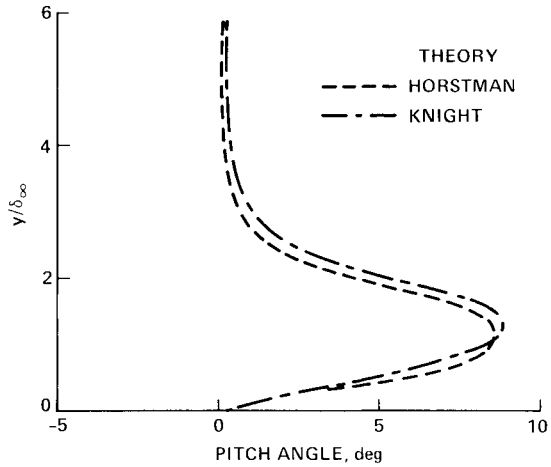

Fig. 12 Computed pitch angle in x direction at $x = 11\delta_\infty$, $z - z_{fin} = 6\delta_\infty$.

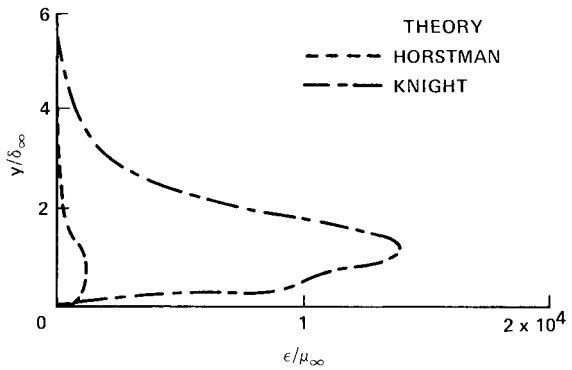

Fig. 13 Computed turbulent eddy viscosity in x direction at $x = 11\delta_\infty$, $z - z_{fin} = 6\delta_\infty$.

Note that it is difficult to define a "local" boundary-layer thickness within the three-dimensional interaction region due to the nonuniformity of the inviscid flow.[10] In Fig. 13, however, the eddy viscosity profiles indicate a significant difference; in particular, the peak values of the turbulent eddy viscosity ϵ differ *by a factor of 14*. It is emphasized that this difference in eddy viscosity between the two models is typical of the profiles within the three-dimensional interaction region. Within the nominal two-dimensional portion of the boundary layer upstream of the interaction, the eddy viscosity profiles are in reasonably close agreement.

It is evident from Figs. 10–13 and the additional numerous profiles studied that the details (i.e., the velocity, pressure, and temperature) of this three-dimensional turbulent interaction are relatively insensitive to the particular turbulence model

employed, with the exception of a small fraction of the boundary layer adjacent to the surface where modest differences are observed in the yaw angle. This implies therefore that the principal elements of the flowfield structure are rotational and inviscid, except within a small portion of the boundary layer adjacent to the wall where the specific details of the turbulence structure are important and may not be fully manifested in either turbulence model. This represents a significant result for three-dimensional interactions, and is notably different from two-dimensional separated shock/boundary-layer interactions wherein the differences between the computed flowfields obtained using algebraic and two-equation turbulence models are significant.[27] There is no reason to expect, however, that the insensitivity to the turbulence model displayed in the three-dimensional sharp fin interaction will necessarily apply to other three-dimensional turbulent interactions.

C. Flowfield Structure of Three-Dimensional Sharp Fin

On the basis of the close agreement between the computed and experimental data, the computed solutions can be utilized to examine the flow structure of the three-dimensional sharp fin interaction. The close similarity of the computed velocity, yaw and pitch angle profiles for the Baldwin-Lomax and Jones-Launder models implies a close agreement in predicted mean streamlines, which was confirmed through detailed comparison of numerous particle traces.

In Figs. 14 and 15, the computed surface skin friction lines obtained using the Baldwin-Lomax and Jones-Launder models are shown. The figures are drawn using the same scale. The lines of coalescence (separation) and divergence (attachment) are indicated. These specific features are in general agreement with the experimental kerosene lampblack visualization as described previously, although the computed lines of coalescence appear further downstream than in the experiment. In particular, the experimental line of coalescence at $z/\delta_\infty = 10$ (the approximate spanwise limit of the experimental kerosene lampblack visualization) is $x_s = -5.7\delta_\infty$, whereas the computed lines of coalescence using the Baldwin-Lomax and Jones-Launder models occur at $x_s = -4.5\delta_\infty$ and $-3.5\delta_\infty$, respectively. These discrepancies represent approximately one and five streamwise grid spacings for the Baldwin-Lomax and Jones-Launder calculations, respectively. Further investigations of three-dimensional turbulent interactions are needed to understand the effects of the turbulence models on the calculated lines of coalescence.

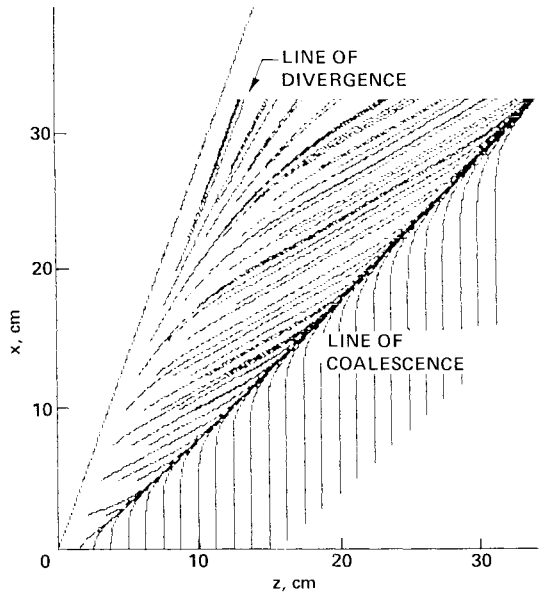

Fig. 14 Computed surface skin friction lines (Baldwin-Lomax).

A series of calculated mean streamlines and surface skin friction lines are displayed in Figs. 16–18, obtained from the computed solution utilizing the Baldwin-Lomax model. In Fig. 16, a series of 12 lines is shown. First, a set of six surface skin friction lines originate from a station upstream of the interaction at spanwise increments equal to δ_∞. These lines define the line of coalescence. Second, a series of six streamlines originate upstream of the interaction at $y = 0.0048\delta_\infty$. These streamlines rise and cross the line of coalescence, and appear to concentrate within a core. In Fig. 17, another series of 12 lines is shown. First, the same set of six surface skin friction lines is drawn to define the line of coalescence. Second, a series of six streamlines originates upstream of the interaction at $y = 0.52\delta_\infty$. These streamlines rise and cross the line of coalescence, and rotate in a counterclockwise direction (as viewed by an observer, located at the leading edge of the

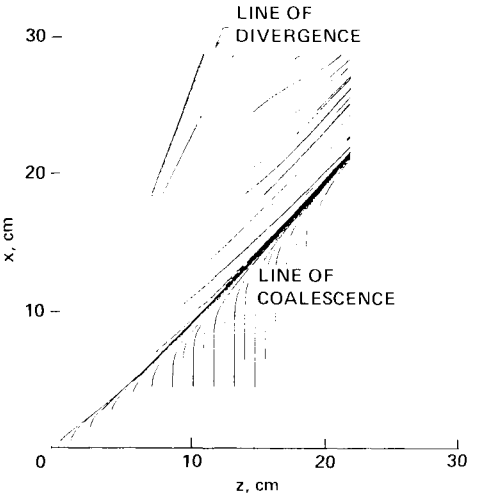

Fig. 15 Computed surface skin friction lines (Jones-Launder).

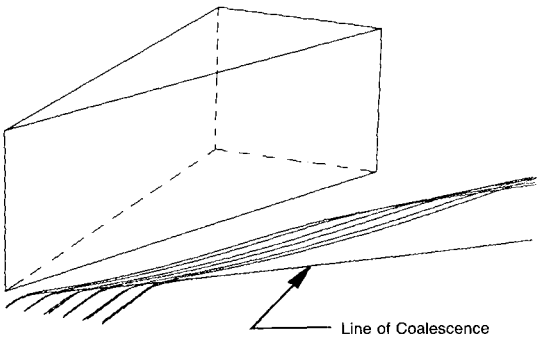

Fig. 16 Computed surface skin friction lines and mean streamlines originating upstream at $y = 0.0048\delta_\infty$.

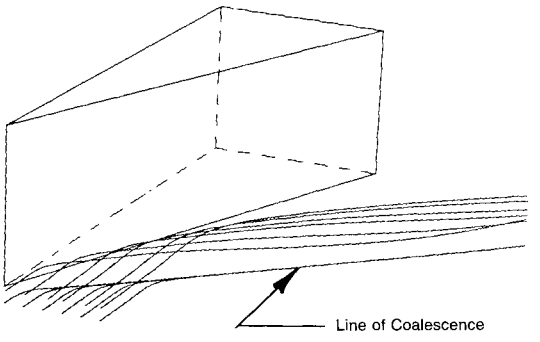

Fig. 17 Computed surface skin friction lines and mean streamlines originating upstream at $y = 0.52\delta_\infty$.

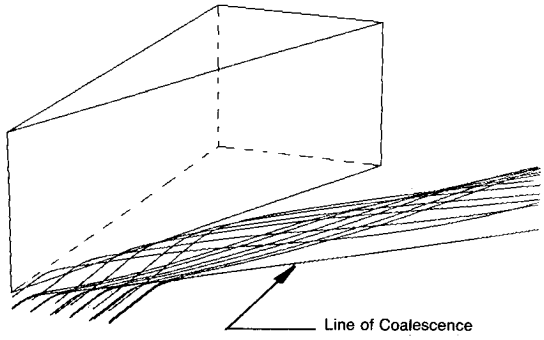

Fig. 18 Computed surface skin friction lines and mean streamlines originating upstream at $y = 0.0048\delta_\infty$ and $0.52\delta_\infty$.

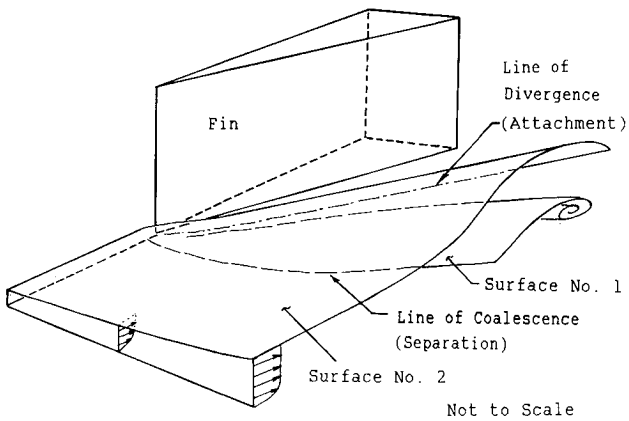

Fig. 19 Mean flowfield structure.

fin, looking along the line of coalescence). The rotational motion brings this higher-energy fluid, originating in the outer portion of the boundary layer, close to the surface. In Fig. 18, the three families are drawn. The streamlines originating at $y = 0.52\delta_\infty$ are observed to rotate counterclockwise around the streamlines originating at $y = 0.0048\delta_\infty$. The low-energy fluid originating near the surface (Fig. 16) rises within the boundary layer. The high-energy fluid originating in the outer portion of the boundary layer (Fig. 17) is swept underneath the lower-energy fluid. The combined effect yields an undershoot in the pitot pressure within the boundary layer (Figs. 3–5).

A general mean flowfield pattern, developed on the basis of the streamline patterns, is displayed in Fig. 19. As suggested by Token,[22] the flowfield structure of the three-dimensional sharp fin at the present conditions is dominated by a large vortical structure. The line of coalescence (separation) defines the origin of the three-dimensional separation surface (surface 1). The line of divergence (attachment) represents the intersection of a second surface (surface 2) with the wall. This second surface extends upstream into the undisturbed flow. The fluid contained between the wall and the second surface becomes the vortical structure, while the fluid above the second surface flows toward the wall and approximately parallel to the fin.

The computed flowfields[12,15] for the three-dimensional sharp fin at Mach 3 for $\alpha_g = 10$ deg and $Re_{\delta\infty} = 3.4 \times 10^5$ and 8.8×10^5 were examined to determine the relevance of the above flowfield structure. A detailed study of flow streamlines indicated that the same structure is applicable. The interaction at $\alpha = 10$ deg and Mach 3, however, is substantially milder, and the vortical structure, although evident in the streamline pattern, is relatively weak. The magnitude of the rotational motion within the vortical structure is substantially less than for $\alpha_g = 20$ deg, as expected from the smaller values of the flow yaw angle.

V. Conclusions

An experimental and theoretical study was performed for the three-dimensional shock wave turbulent boundary-layer interaction generated by a sharp fin at Mach 3 for a fin angle $\alpha_g = 20$ deg and Reynolds number $Re_{\delta\infty} = 9 \times 10^5$. This study extends previous experimental and theoretical investigations of the three-dimensional sharp fin interaction to stronger interactions. Two separate theoretical approaches or "models" were employed, both of which utilize the three-dimensional compressible Navier-Stokes equations. The theoretical approach of Knight employs the algebraic turbulent eddy viscosity model of Baldwin and Lomax, and the theoretical model of Horstman employs the two-equation turbulence model of Jones and Launder coupled with the wall function model of Viegas and Rubesin. The principal conclusions are:

1) The computed surface pressure, surface streamlines, pitot pressure, and yaw angle profiles are observed in good agreement with the experimental data, thereby confirming the efficacy of the theoretical approaches which were previously validated for the three-dimensional sharp fin configuration at Mach 3 for smaller α_g (i.e., weaker interactions).

2) The three-dimensional velocity fields computed by both models are in close agreement, as indicated by a detailed evaluation of x-component velocity, pitch, and yaw angle profiles. Modest differences were observed in the computed yaw angle in a narrow region of the boundary layer adjacent to the wall. The turbulent eddy viscosity profiles, however, differ significantly within the three-dimensional interaction. This result implies that the overall structure of this three-dimensional sharp fin interaction is insensitive to the turbulence model, except within a small portion of the boundary layer adjacent to the surface where the turbulence structure is important and may not be fully manifested in either turbulence model. Detailed experimental data on surface skin friction and heat transfer are needed to elucidate the differences in the turbulence models near the surface. Overall, the principal elements of the flowfield structure are rotational and inviscid, except near the wall as indicated.

3) The calculated flowfields display a prominent vortical structure associated with the shock/boundary-layer interaction in agreement with the flowfield models of Token,[22] and Kubota and Stollery.[5] A three-dimensional surface of separation emanates from the line of coalescence (separation), and spirals into the vortical center. A second surface, emanating from upstream, intersects the wall at the line of divergence (attachment), and defines the extent of the fluid entrained into the vortical structure.

VI. Acknowledgments

This research was sponsored by the Air Force Office of Scientific research under AF Grant 82-0040 and Contract 150-6490, monitored by Dr. James Wilson, and the NASA Ames and NASA Langley Research Centers.

References

[1]Settles, G. and Dolling, D., "Swept Shock Wave-Boundary Layer Interactions," AIAA Progress in Astronautics and Aeronautics, Sept. 1986.

[2]Stanbrook, A., "An Experimental Study of the Glancing Interaction Between a Shock Wave and a Boundary Layer," British ARC CP-555, July 1960.

[3]McCabe, A., "The Three-Dimensional Interaction of a Shock Wave with a Turbulent Boundary Layer," *The Aeronautical Quarterly*, Vol. 17, 1966, pp. 231–252.

[4]Law, C., "Three-Dimensional Shock Wave/Turbulent Boundary Layer Interactions at Mach 6," ARL-TR-75-0191, June 1975.

[5]Kubota, H. and Stollery, J., "An Experimental Study of the Interaction Between a Glancing Shock Wave and a Turbulent Boundary Layer," *Journal of Fluid Mechanics*, Vol. 116, March 1982, pp. 431–458.

[6]Zheltovodov, A., "Regimes and Properties of Three-Dimensional Separation Flows Initiated by Skewed Compression Shocks," *Zhurnal*

Prikladnoi Mekhaniki i Tekknicheskoi Fiziki, No. 3, May–June 1982, pp. 116–123.

[7]Dolling, D., "Upstream Influence in Sharp Fin-Induced Shock Wave Turbulent Boundary-Layer Interactions," *AIAA Journal*, Vol. 21, Jan. 1983, pp. 143–145.

[8]Goodwin, S., "An Exploratory Investigation of Sharp-Fin Induced Shock Wave/Turbulent Boundary Layer Interactions at High Shock Strengths," MS Thesis, Dept. Aerospace and Mechanical Engineering, Princeton Univ., 1984.

[9]Peake, D., "Three Dimensional Swept Shock/Turbulent Boundary Layer Separations with Control by Air Injection," Aero Rept. LR-592, National Research Council, Canada.

[10]Oskam, B., Vas, I., and Bogdonoff, S., "Mach 3 Oblique Shock Wave/Turbulent Boundary Layer Interactions in Three Dimensions," AIAA Paper 76-336, Jan. 1976.

[11]McClure, W. and Dolling, D., "Flowfield Scaling in Sharp Fin-Induced Shock Wave Turbulent Boundary Layer Interaction," AIAA Paper 83-1754, July 1983.

[12]Horstman, C. and Hung, C., "Computation of Three-Dimensional Turbulent Separated Flows at Supersonic Speeds," AIAA Paper 79-0002, Jan. 1979.

[13]Knight, D., "A Hybrid Explicit-Implicit Numerical Algorithm for the Three-Dimensional Compressible Navier-Stokes Equations," *AIAA Journal*, Vol. 22, Aug. 1984, pp. 1056–1063.

[14]Knight, D., "Numerical Simulation of 3-D Turbulent Boundary Layer Interaction Generated by a Sharp Fin," *AIAA Journal*, Vol. 23, Dec. 1985, pp. 1885–1891.

[15]Knight, D., "Modelling of Three-Dimensional Shock Wave Turbulent Boundary Layer Interactions," *Lecture Notes in Physics*, Vol. 230, Springer-Verlag, New York, 1985, pp. 177–201.

[16]Knight, D., Horstman, C., Shapey, B., and Bogdonoff, S., "The Flowfield Structure of the 3-D Shock Wave-Boundary Layer Interaction Generated by a 20 deg Sharp Fin at Mach 3," AIAA Paper 86-0343, Jan. 1986.

[17]Escudier, M., "The Distribution of the Mixing Length in Turbulent Flows Near Walls," Mech. Engr. Dept., Imperial College, London, Rept. TWF/TN/1, 1965.

[18]Horstman, C., private communications, June 1984, July 1984, Nov. 1984.

[19]Jones, W. and Launder, B. "The Prediction of Laminarization with a Two-Equation Model of Turbulence," *International Journal of Heat and Mass Transfer*, Vol. 15, 1972, pp. 301–304.

[20]Baldwin, B. and Lomax, H., "Thin Layer Approximation and Algebraic Model for Separated Flows," AIAA Paper 78-257, Jan. 1978.

[21]Horstman, C., "Computation of Sharp-Fin-Induced Shock Wave/Turbulent Boundary Layer Interactions," AIAA Paper 86-1032, May 1986.

[22]Token, K., "Heat Transfer Due to Shock Wave/Turbulent Boundary Layer Interactions on High Speed Weapons Systems," AFFDL-TR-74-77, 1974.

[23]Settles, G. and Teng, H.-Y., "Flow Visualization of Separated 3-D Shock Wave/Turbulent Boundary Layer Interactions," *AIAA Journal*, Vol. 21, March 1983, pp. 390–397.

[24]Viegas, J., Rubesin, M., and Horstman, C., "On the Use of Wall Functions as Boundary Conditions for Two-Dimensional Separated Compressible Flows," AIAA Paper 85-0180, Jan. 1985.

[25]Horstman, C., "A Computational Study of Complex Three-Dimensional Compressible Turbulent Flow Fields," AIAA Paper 84-1556, June 1984.

[26]MacCormack, R., "Numerical Solution of the Interaction of a Shock Wave with a Laminar Boundary Layer," *Lecture Notes in Physics*, Vol. 8, 1971, pp. 151–163.

[27]Coakley, T., Viegas, J., and Horstman, C., "Evaluation of Turbulence Models for Three Primary Types of Shock Separated Boundary Layers," AIAA Paper 77-692, June 1977.